Self-Assembled Nanoparticles with Dual Effects of Passive Tumor Targeting and Cancer-Selective Anticancer Effects

*Young-Wook Won, Sun-Mi Yoon, Kwang Suk Lim, and Yong-Hee Kim**

Nanoparticular drug delivery systems may help to overcome the limitations of conventional chemotherapy. They have been reported to improve the specificity of distribution, the bioavailability, and the solubility of drugs, as well as the duration of drug efficacy, and helping to overcome multidrug resistance. Although various polymeric nanoparticles have been developed for delivery of anticancer agents, most nanoparticles still focus on solubilizing drugs, improving targeting ability, and reducing side effects. In particular, targeting to the tumor is typically improved through passive or active targeting. Despite great achievements in both strategies, yet to be resolved are issues of toxicity in normal cells and enhancement of tumor-specificity. A new approach combining the dual strategies of passive tumor targeting and cancer-selective efficacy is proposed. Recombinant human gelatin conjugated with lipoic acid (rHG-LA) developed in this study forms nanoparticles spontaneously in aqueous solution and encapsulates alpha-tocopheryl succinate (α-TOS), a well-known cancer-selective apoptosis-inducing agent, within a hydrophobic core during the self-assembly. This study describes the promising applicability of α-TOS-loaded rHG-LA nanoparticles with passive targeting ability and cancer-specificity.

1. Introduction

Polymeric nanoparticles can encapsulate hydrophobic anticancer drugs and carry the drugs to the tumor region via the enhanced permeability and retention (EPR) effect.[1–3] Exploitation of these properties for drug delivery provides a basis for developing nanoparticular drug-delivery systems that can be utilized for anticancer agents. Recently, it has been widely accepted that passive targeting based on the EPR effect is not enough to eradicate the side effects of cytotoxic drugs and exert their anticancer efficacy selectively in cancer cells.[4,5] Active targeting is therefore being widely studied to overcome the limitations of passive targeting. Despite the great achievements in this area, only slight improvements have so far been made in improving the anticancer efficacy and reducing the side effects. Consequently, a new approach is necessary for successful cancer nanotherapy.

Dr. Y.-W. Won, S.-M. Yoon, K. S. Lim, Prof. Y.-H. Kim
Department of Bioengineering
Institute for Bioengineering and Biopharmaceutical Research
Hanyang University
17, Haengdang-dong, Seongdong-gu,
Seoul, 133-791, Republic of Korea
E-mail: yongheekim@hanyang.ac.kr

DOI: 10.1002/adfm.201101979

The primary disadvantage of conventional chemotherapeutics is dose-limiting cytotoxicity, because typically the aim is to destroy rapidly dividing cells through direct drug-induced toxicity.[6] The nanoparticular drug-delivery systems developed for the purpose of passive or active targeting have shown a moderate improvement in anticancer efficacy and reduction of side effects.[7,8] To further enhance the tumor-specificity of the cancer nanotherapeutics, cancer cell-selective anticancer agents have emerged as alternatives to the conventional cytotoxic drugs.[9] Among various cancer cell-specific agents, alpha-tocopheryl succinate (α-TOS), one of the vitamin E analogues, is known to trigger massive apoptosis in various tumor types, arrest the cell cycle, and disrupt the autocrine signaling pathways essential for tumor growth.[10,11] α-TOS is composed of three domains: the functional, signaling, and hydrophobic domains. The succinyl group in the functional domain plays a crucial role in cancer cell-specific apoptosis through the generation of reactive oxygen species (ROS) triggering the apoptotic pathway.[12] Despite the importance of the succinyl group, it is easily cleaved through esterase-dependent hydrolysis, through which α-TOS is converted into α-TOH, a non-apoptotic analogue of vitamin E.[13] α-TOS selectively kills cancer cells with relatively low toxicity toward normal cells because normal cells are sufficient to cleave α-TOS, while cancer cells lack sufficient esterase activity.[14,15] Therefore, α-TOS induces ROS accumulation and selective apoptosis in various cancer cell lines. Despite the potential value of α-TOS, the loss of anticancer activity in physiological environments and its insolubility in water have remained as the main obstacles for use.

Recombinant human gelatin (rHG) is known to be a good biomaterial with advantages over animal-derived gelatin, which is widely used as a stabilizer and capsule material in the pharmaceutical industry.[16] Although gelatin derived from porcine or bovine tissues is more biocompatible and biodegradable than most synthetic polymers, they may induce anaphylaxis and carry prion diseases.[17,18] In addition, heterogeneity in molecular weight may result in a wide range of nanoparticle sizes when it is used for manufacturing nanoparticles.[19] On the other hand, rHG shows desirable properties for nanoparticle fabrication and the targeted delivery of anticancer drugs in terms of uniform particle size resulting from the homogeneity in molecular weight.[20] For hydrophobic drug delivery, a modification of

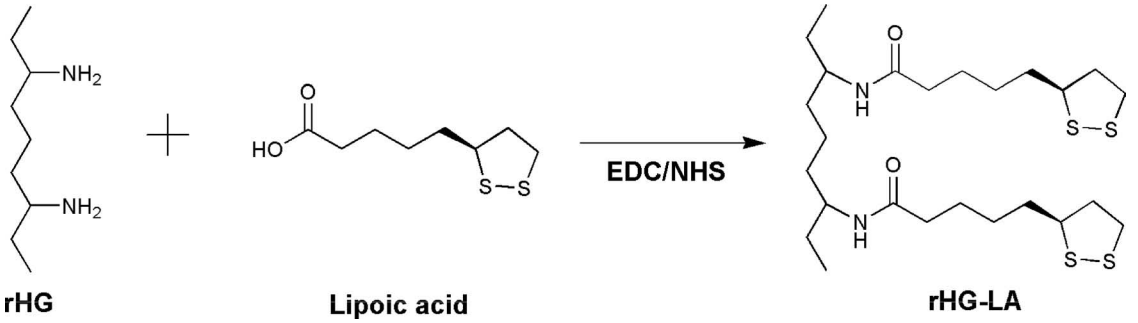

Figure 1. Schematic representation of the conjugation. The conjugate of rHG-LA was formed through EDC/NHS-activated amide bond.

rHG with hydrophobic molecules is necessary because the hydrophilic nature of rHG limits its use in water-soluble drugs.

Lipoic acid (LA), a sulfur-containing fatty acid found within every cell of the body, serves as a cofactor in energy metabolism and various transfer reactions. Due to the abundance in the body, LA is appropriate to use as a hydrophobic molecule for the modification of rHG into an amphiphilic polymer (rHG-LA). Within the hydrophobic core of the rHG-LA nanoparticle, a hydrophobic drug can be encapsulated, protecting it against degradation, and efficiently delivered to the target site, where it is released in a highly available form. Furthermore, within tumor cells, the vicinal thiol groups of LA may be largely reduced through reaction with GSH because the cellular GSH level in cancer cells has been found to be higher than that in a normal cell.[21] Thus, the increase in polarity may lead to the nanoparticle disassembly facilitating the drug release.

In this study, we propose a new direction for cancer nanotherapy representing dual effects of cancer-selective apoptosis and passive targeting. We demonstrate the capability of rHG-LA nanoparticles for delivering α-TOS to the tumor site and the cancer cell-specific apoptosis in vitro. The rHG-LA nanoparticles are able to protect α-TOS against hydrolysis, resulting in enhanced anticancer efficacy, and to deliver it selectively to the tumor region through the EPR effect. Our findings suggest that the development of nanoparticular drug delivery systems encapsulating cancer-selective agents is a promising strategy for cancer therapy in terms of tumor targeting ability and cancer-selectivity.

2. Results and Discussion

Nanoparticular drug delivery systems for anticancer agents have focused on the use of cytotoxic chemotherapeutics and passive or active targeting is a main purpose of development of nanoparticles. However, they still need to be further improved to enhance the anticancer efficacy and reduce the dose-limiting toxicity, because the tumor targeting ability is insufficient and the intrinsic toxicity of chemotherapeutics has not been fully lost. One solution would be the use of cancer cell-selective anticancer agents. Although various cancer-specific agents have shown promising therapeutic efficacy, no nanoparticular drug delivery systems utilized for those agents have been reported. It is expected that nanoparticles encapsulating cancer-specific agents will have the benefits of passive targeting, protecting the agents under physiological conditions, as well as cancer-specificity.

2.1. Characterization of rHG-LA Nanoparticles

rHG was modified into amphiphilic polymer by the introduction of LA, used as the hydrophobic molecule for the amphiphilic modification of polymers (**Figure 1**). LA, an organosulfur compound derived from octanoic acid, includes a carboxylic acid and a dithiolane ring which contains two vicinal sulfur atoms (at C6 and C8) attached through a disulfide bond.[22] The EDC/NHS reaction easily forms an amide bond between the carboxyl group in LA and the amine group in rHG. Fourier transform infrared (FT-IR) spectroscopy was used to confirm the conjugation and a TNBS assay was performed to determine the substitution degree.[16] Typical FT-IR spectra for rHG, LA, and rHG-LA conjugate are shown in **Figure 2**. In the spectrum of rHG-LA, a new peak that represents the amide bond formed through rHG-LA

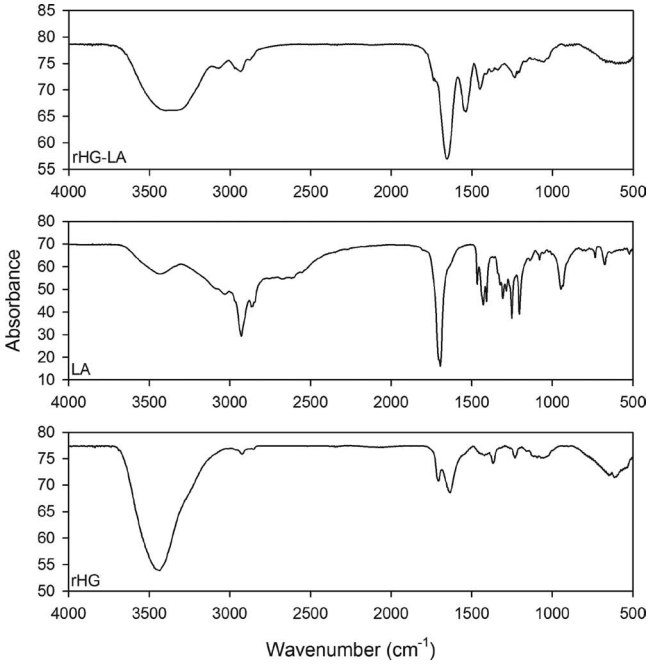

Figure 2. FT-IR spectra of rHG-LA conjugates, LA, and rHG. The new absorption band at 1530 cm^{-1} is associated with the amide band.

conjugation was observed at 1530 cm^{-1}, while this new peak was not observed in either rHG or LA, demonstrating successful conjugation of rHG-LA as per our hypothesis. The quantitative analysis of the substitution degree revealed that approximately 20% of the free amine content existed in the rHG-LA conjugates, indicating that the rHG-LA conjugation achieved around 80% substitution. Size-exclusion chromatography (SEC) performed to observe a change in the molecular weight after conjugation showed an elution time shift from 7.5 to 6.5 min. The typical elution times for rHG-LA and rHG were found to be 6.5 and 7.5 min, respectively, under test conditions, confirming that rHG was conjugated with LA because the shorter elution time for rHG-LA indicates an increase in molecular weight.

The self-assembly of rHG-LA conjugates in an aqueous solution was confirmed by measuring the critical aggregation concentration (CAC) of the conjugates determined using the fluorometry probe. DPH was co-incubated with rHG-LA conjugates at various concentrations, with the absorbance spectrum of DPH monitored. Mean absorbance values were calculated. As the rHG-LA aggregates in the aqueous solution, the hydrophobic DPH intercalates into the inner hydrophobic region of the aggregates, resulting in a decisive shift in DPH absorbance. CAC was determined based on the threshold concentration of self-assembling aggregates at which the shift in DPH absorbance occurs. A plot of DPH absorbance versus the logarithm of the rHG-LA nanoparticle concentration (**Figure 3**a) yielded

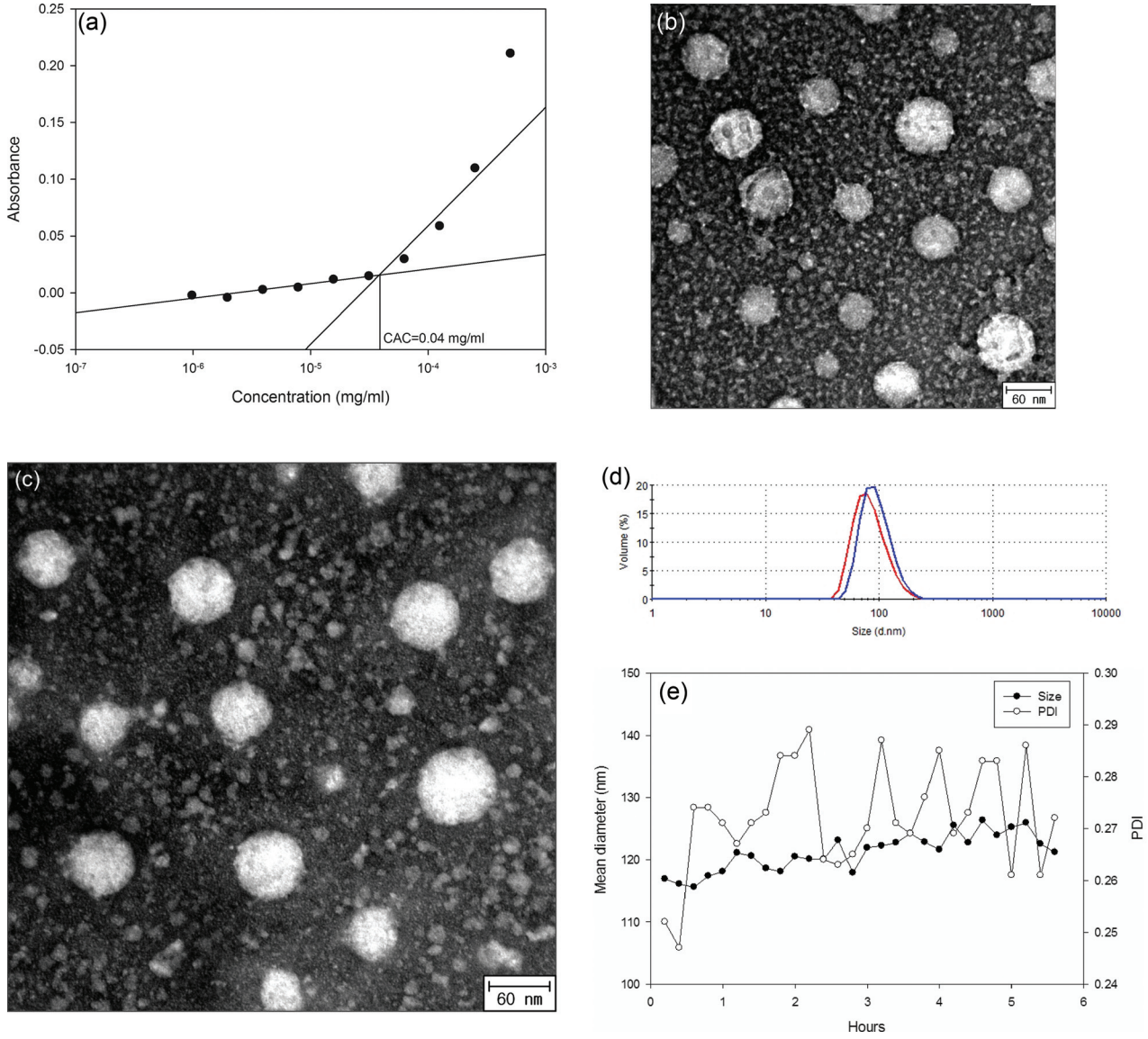

Figure 3. a) Fluorometry probe-based CAC value of the rHG-LA conjugates (CAC: approximately 0.04 mg mL^{-1}). TEM microscopy images of: b) unloaded rHG-LA and c) α-TOS/rHG-LA nanoparticles. d) Volume-based size distribution of the rHG-LA nanoparticles (red: distribution in water; blue: distribution in phosphate buffered saline (PBS)). e) Nanoparticle stability in the presence of salt and serum protein. The rHG-LA conjugates formed spherical nanoparticles ranging from 40 to 100 nm in the aqueous solution.

a CAC value of 0.04 mg mL^{-1}. The shift in DPH absorbance indicates incorporation of the probe into a newly formed hydrophobic environment, confirming the formation of self-assembly, as required for an effective hydrophobic drug carrier. In addition, the CAC value may indicate the minimum amount of rHG-LA conjugates required for systemic administration because the concentration of rHG-LA is diluted in blood; therefore, the aggregates may disassemble upon injection, when the final concentration of rHG-LA conjugates is lower than the CAC.[23,24]

Transmission electron microscopy (TEM) analysis confirmed the types of nanostructure formed via the self-assembly of rHG-LA conjugates in the aqueous environment. As shown in Figure 3b, the rHG-LA conjugates formed spherical nanoparticles with a homogenous size distribution without aggregation and distributed in the range from 40 to 100 nm in diameter. The size distribution analyzed using DLS showed that approximately 95% of the rHG-LA nanoparticles existed in the range from 45 to 105 nm in diameter in water, suggesting no difference in the TEM and DLS analysis. In order to confirm whether drug-loading affects the self-assembly of rHG-LA, the characteristics of α-TOS-loaded rHG-LA (α-TOS/rHG-LA) nanoparticles were examined using TEM and DLS. Figure 3c shows negligible differences in the nanoparticle structure in comparison with Figure 3b and the mean diameters of each nanoparticles were determined to be 96 ± 6 nm for rHG-LA and 103 ± 7 nm for α-TOS/rHG-LA, with PDI values of 0.154 ± 0.041 and 0.193 ± 0.015, respectively. The size and zeta potential were measured in PBS in order to determine the nanoparticle stability in salt-containing solution. The size distributions of α-TOS/rHG-LA in water and PBS were shown in Figure 3d and the size and zeta potential in PBS were 123.6 ± 16.7 nm with a PDI value of 0.258 ± 0.28, and −1.42 ± 0.35 mV with a PDI value of 0.233 ± 0.046, respectively. To examine the long-term stability of the nanoparticles in the presence of serum protein, the mean diameter was determined for 6 h in the presence of human serum albumin (HSA)-containing PBS. No difference in the size was observed during the test period, demonstrating that no aggregation and no interaction with the serum protein occurred. These data demonstrate that rHG-LA conjugates spontaneously assemble into the nanoparticles in an aqueous environment, the drug loading has no influence on the nanoparticle structure, and the nanoparticles are stable in the presence of both salt and serum protein.

2.2. In Vitro Release of α-TOS from the rHG-LA Nanoparticles

The α-TOS has to be released in a controlled manner from the rHG-LA nanoparticles for the therapeutic purposes. To examine the in vitro release of α-TOS, α-TOS/rHG-LA nanoparticles were incubated in a dialysis membrane under heating and shaking, and the released α-TOS was quantified using HPLC. As shown in **Figure 4**a, the nanoparticles released α-TOS, reaching around 40% completion after 6 h and around 50% in the first day. The first phase of release was completed within 6 h and this value was considered as an initial burst. After 6 h, the release pattern followed by a second phase showing slow sustained release. The biphasic release pattern showed approximately 80% release of α-TOS and reached a steady state after 4 d. It is widely accepted that the initial moderately fast release and the later sustained release contribute a rapid drug effect on the tumor and a continuous anticancer efficacy, respectively, both of which lead to good drug efficacy. The release kinetic needs to be optimized to exert a maximized drug efficacy when other kinds of hydrophobic agents are delivered by rHG-LA nanoparticles. Changing rigidity of nanoparticles is typical method to control the release pattern and the hydrophobic domain plays crucial role in the rigidity, suggesting that the release kinetic may be different when the substitution degree of LA is changed. In addition, the release kinetic is associated with both dissolution and diffusion based on the Noyes-Whitney law of dissolution and Fick's first law of diffusion, regardless of the mechanism of drug release.[25]

The succinyl group in the C6 position of the chromanol ring promotes cancer cell-specific apoptosis; however, the ester bond through which the succinyl group is connected with the chromanol ring is easily hydrolyzed into α-TOH. Therefore, the stability of α-TOS has to be preserved inside the nanoparticles during the release period. To confirm the stability of α-TOS, stability-indicating HPLC was performed after the release.[26,27] As shown in Figure 4b, the released α-TOS was eluted at the same time point as the control, which exhibited an elution time of 8.8 min under the test conditions. On the other hand, free α-TOS without rHG-LA nanoparticles incubated under the same test conditions was eluted at different time points with other peaks representing changes in structure, suggesting that the α-TOS was hydrolyzed in the absence of nanoparticles. These data reveal that rHG-LA nanoparticles sufficiently protect α-TOS against the hydrolysis; hence, α-TOS conserves its structure necessary to exert the cancer cell-selective anticancer efficacy.

2.3. Intracellular Localization of rHG-LA Nanoparticles

The rHG-LA nanoparticles have to be internalized and localized in cytoplasm, in which the α-TOS-mediated cancer cell-specific apoptotic mechanism occurs. The cellular uptake of the rHG-LA nanoparticles was examined in SCC-7 cells. To visualize the cellular uptake of rHG-LA nanoparticles, the rHG-LA was labeled with Cy5.5 and cell nuclei were counter-stained with DAPI. **Figure 5**a shows a time-dependent cellular uptake behavior of the Cy5.5-labeled rHG-LA nanoparticles. Observations using a CLSM showed a time-dependent increase in the internalization of rHG-LA nanoparticles, indicating that the cells were able to efficiently uptake the rHG-LA nanoparticles. The rHG-LA nanoparticles rapidly initiated to internalize into the cells, continuously localized in the cytoplasm, and well dispersed in the cytoplasm; thus, the α-TOS might be able to exert the anticancer effects successfully upon release. The cellular uptake was further quantitatively analyzed using FACS. As shown in Figure 5b and c, the nanoparticle internalization was approximately 20% and 50% at 30 min and 1 h, respectively, and the uptake reached a plateau near to 100% at 6 h.

2.4. In vitro Anticancer Efficacy of α-TOS/rHG-LA Nanoparticles

The cancer cell-selective apoptotic effects of α-TOS/rHG-LA nanoparticles were evaluated in various types of normal and

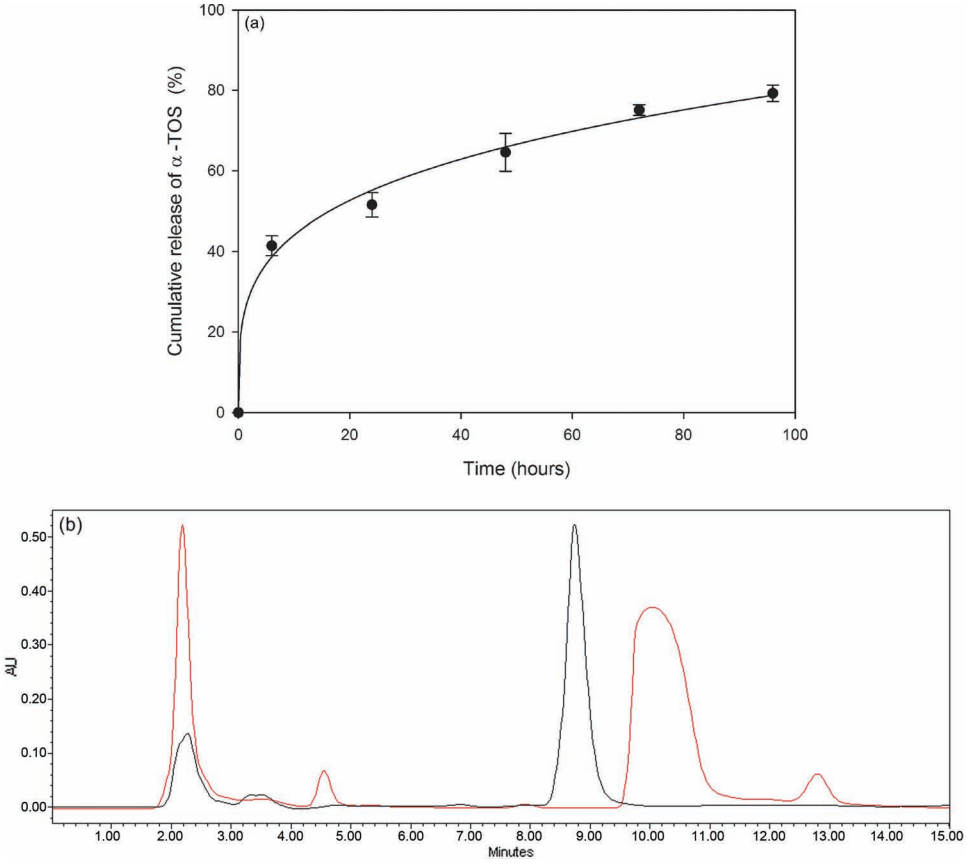

Figure 4. a) In vitro release profile of α-TOS from the rHG-LA nanoparticles at pH 7.4 and 37 °C under shaking at 100 rpm (data expressed as mean ± standard deviation (S.D.) of three-independent experiments with five replicates). b) Stability of the α-TOS (black: with rHG-LA; red: without rHG-LA) after 4 d of incubation under test conditions. The rHG-LA protected α-TOS during the test period and the released α-TOS was eluted at 8.8 min, where is same time point as the typical elution time of α-TOS under the HPLC condition, whereas free α-TOS showed three peaks at different elution time points.

cancer cells. The difference in esterase activity is a major factor for cancer cell-selective apoptosis because the esterase that hydrolyzes α-TOS is maintained at a low level in cancer cells, whereas normal cells retain a relatively high level of esterase activity; therefore, degradation of α-TOS is moderate in cancer cells.[28–30] The unconverted α-TOS in cancer cells induces mitochondria-mediated apoptosis, whereas the hydrolyzed α-TOH in normal cells exhibits no apoptotic effects. As shown in **Figure 6**, the α-TOS/rHG-LA nanoparticles had significant cytotoxicity in cancer cell lines, whereas no cytotoxic effect was observed in normal cell lines. Although the unloaded rHG-LA nanoparticles are non-toxic, the encapsulated α-TOS retains potency and exerts significant cytotoxicity upon release from the nanoparticles. In this experiment, cancer cells treated with α-TOS/rHG-LA nanoparticles showed a slight increase in the half-maximal inhibitory concentration (IC50) in comparison with that treated with free α-TOS due in part to the incomplete release of α-TOS from the nanoparticles. Although the drug-loaded nanoparticles applied to the cultures contained an amount of α-TOS equivalent to that of the free α-TOS, the nanoparticles released only around 60% of their load within 48 h (Figure 4a). The nanoparticle-treated cultures were therefore exposed to an α-TOS concentration that was 40% lower than that in cells treated with free α-TOS; accordingly, the cytotoxic effect was reduced. Taken together, the loaded α-TOS was protected inside the rHG-LA nanoparticles, thereby the α-TOS/rHG-LA nanoparticles were capable of inducing cancer cell-selective toxicity after α-TOS release in the cytoplasm.

2.5. In Vivo Anticancer Efficacy of α-TOS/rHG-LA Nanoparticles

The advantages of using nanoparticles for cancer therapy mostly rely on the enhanced anticancer efficacy and reduced side effects due to the EPR effect. Although passive targeting based on the EPR effect could increase the accessibility to the tumor and the local concentration of the anticancer drug in the tumor region, the drug also accumulates in normal tissues. It is possible that the accumulated drug in normal tissues may cause side effects, even though the side effects are relatively low compared to those of the injection formulation without nanoparticles. Cancer cell-selective α-TOS/rHG-LA nanoparticles further reduce the potent toxicity in the normal cells. The rHG-LA accumulates at high levels at the tumor site via EPR,

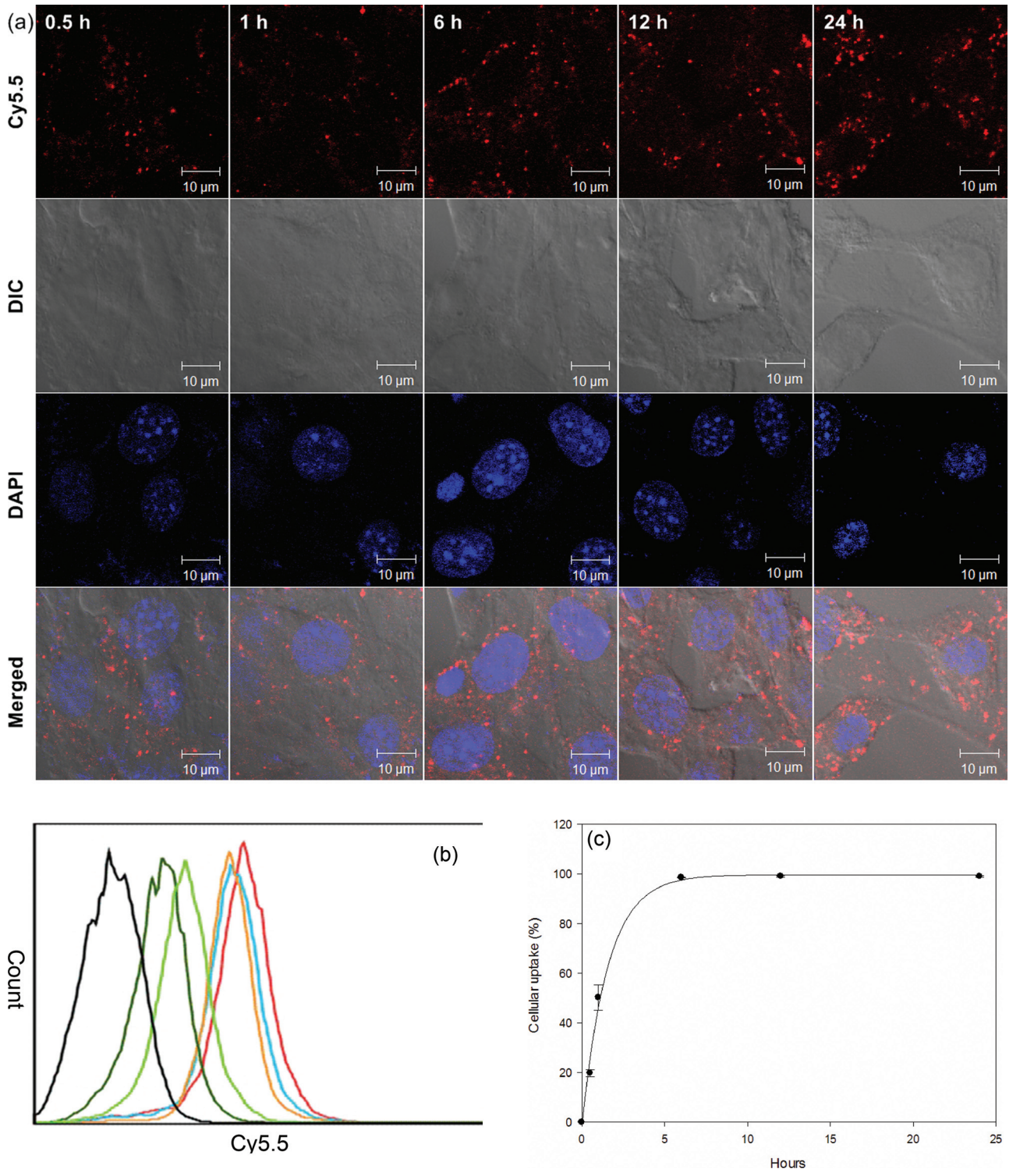

Figure 5. Cellular uptake and intracellular distribution of the rHG-LA nanoparticles visualized using: a) CLSM, b) FACS, and, c) quantitative analysis. The rHG-LA nanoparticles were labeled with Cy5.5 (red), cell morphologies are shown in the DIC image (gray), and the nuclei were counter-stained with DAPI (blue). The cellular uptake was increased as an increase in time (black: control, dark green: 0.5 h, light green: 1 h, orange: 6 h, blue: 12 h, and red: 24 h).

through which the local concentration of α-TOS is increased, and the non-apoptotic effects of α-TOS in normal cells result in no severe side effects when they are accumulated in normal tissues. As shown by in vitro study, the low toxicity of α-TOS/rHG-LA nanoparticles observed in a kidney cell line reveals that the formulation may be non-toxic to the other organs,

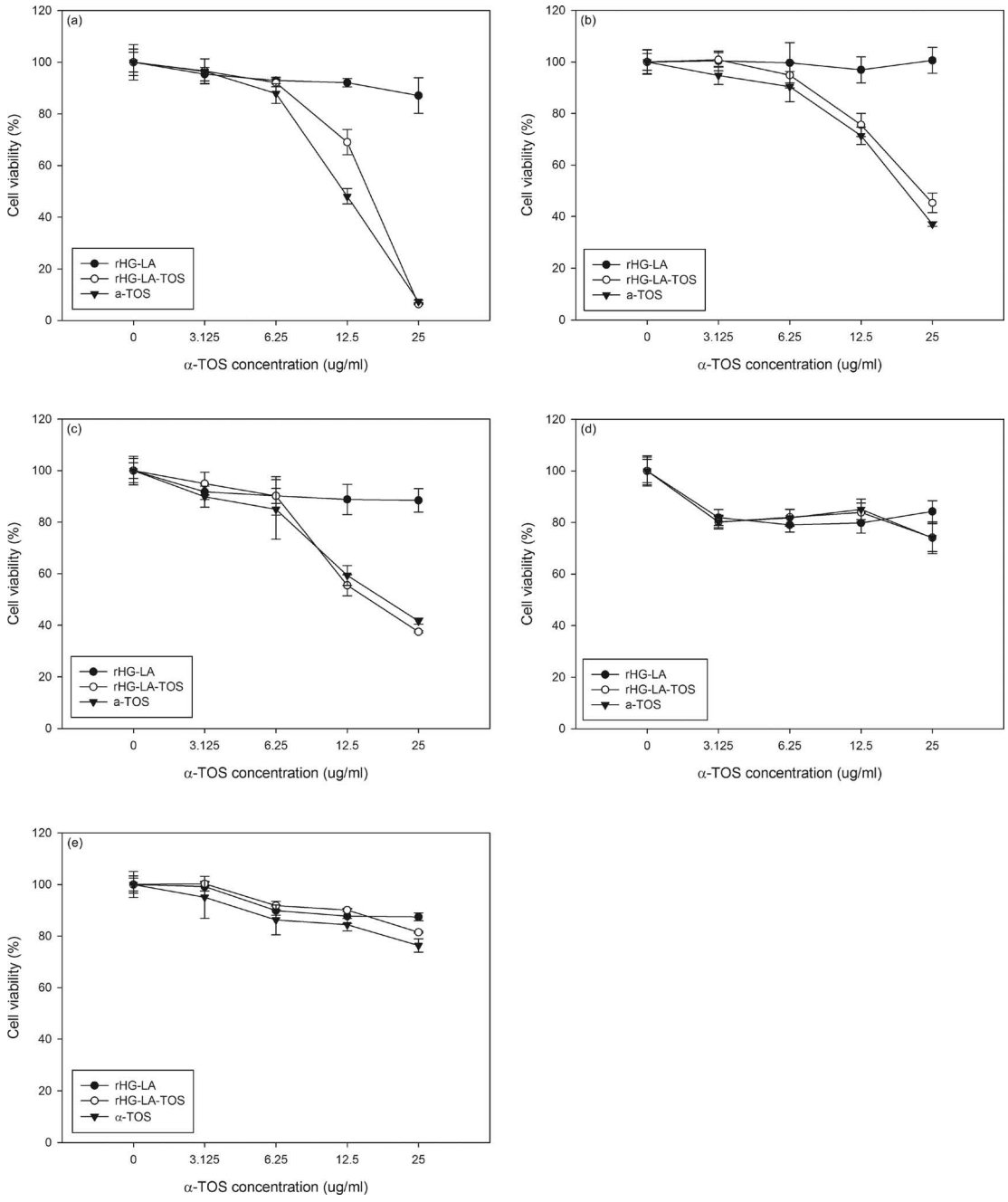

Figure 6. Cytotoxicities of the α-TOS/rHG-LA nanoparticles in cancer cell lines and normal cell lines. Anticancer effects of the nanoparticles were examined in three types of cancer cells, a) SCC-7 (IC50: around 12 μg mL^{-1} of α-TOS), b) A549 (IC50: around 20 μg mL^{-1} of α-TOS), and, c) MCF-7 (IC50: approximately 18 μg mL^{-1} of α-TOS), and two normal cells, d) 3T3-L1, and, e) HEK 293. Data are expressed as mean ± S.D. of three independent experiments with four replicates. Equivalent amounts of α-TOS were treated to the cells in the groups of free α-TOS and α-TOS/rHG-LA nanoparticles and same amounts of rHG-LA used as a vehicle for α-TOS were added to the cells.

even though they are taken up by normal cells such as kidney and liver upon systemic administration. This is one of the major advantages of the present system over the conventional nanoparticle-based carriers developed for anticancer agents.

The anticancer effects of α-TOS/rHG-LA nanoparticles and unloaded nanoparticles were evaluated in a mouse tumor model. Individual groups of mice were injected intravenously with PBS, free α-TOS, or α-TOS/rHG-LA at an equivalent dose of 10 mg kg^{-1} α-TOS and with unloaded rHG-LA nanoparticles. The tumor volumes were measured at various times after these injections. The α-TOS/rHG-LA nanoparticle-treated group developed smaller tumors than those in the group treated with free α-TOS. As shown in **Figure 7**, tumor volumes increased to 1000 mm^3 in the α-TOS/rHG-LA group, 1500 mm^3 in the

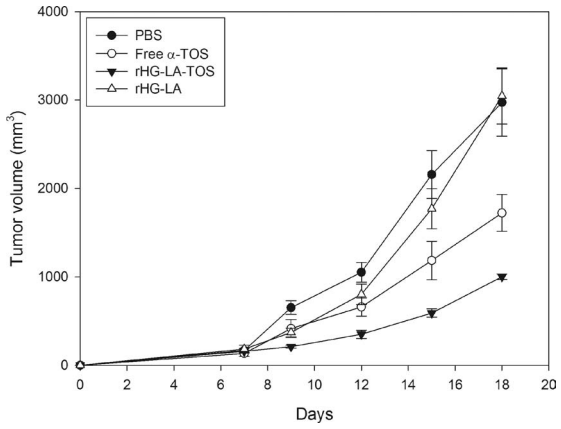

Figure 7. Anticancer effects of the α-TOS/rHG-LA nanoparticles in mouse tumor model. After 7 d of tumor inoculation, the mice were randomly separated into four groups and PBS, free α-TOS, α-TOS/rHG-LA, and rHG-LA were injected intravenously at the α-TOS dose of 10 mg kg^{-1} (data expressed as mean ± standard error (S.E.), $n = 5$).

free α-TOS group, and 3000 mm^3 in the groups of PBS and rHG-LA at day 18. The smaller tumor size in the α-TOS/rHG-LA treatment group compared to that in the free α-TOS group indicates that rHG-LA nanoparticles improved the α-TOS's anticancer effect through passive targeting and protection against hydrolysis.

2.6. Tumor Targeting Ability of rHG-LA Nanoparticles

We hypothesized that intravenous injection of the rHG-LA nanoparticles could achieve in vivo tumor-specific targeting through the EPR effect. To confirm whether this occurred, we assessed the biodistribution of Cy5.5-labeled rHG-LA nanoparticles in the whole body using a non-invasive live-animal imaging technique. As shown in **Figure 8**a, rHG-LA nanoparticles accumulated to a significant extent in the tumor, with the highest accumulations detected 12 h after administration. The accumulation profile of rHG-LA nanoparticles visualized using NIR fluorescence intensity is consistent with tumor-specific targeting as a result of the EPR effect. Figure 8b shows the distribution of rHG-LA nanoparticles in major organs, including the liver, lung, kidney, spleen, heart, and muscle, as well as in the tumor, 12 h after injection of Cy5.5-labeled rHG-LA nanoparticles. The data show a significant accumulation of rHG-LA nanoparticles in the tumor, with the highest fluorescent intensity observed in the tumor compared to those of the other tissues. As shown in Figure 8c, the tumor-to-background ratio (TBR) increased up

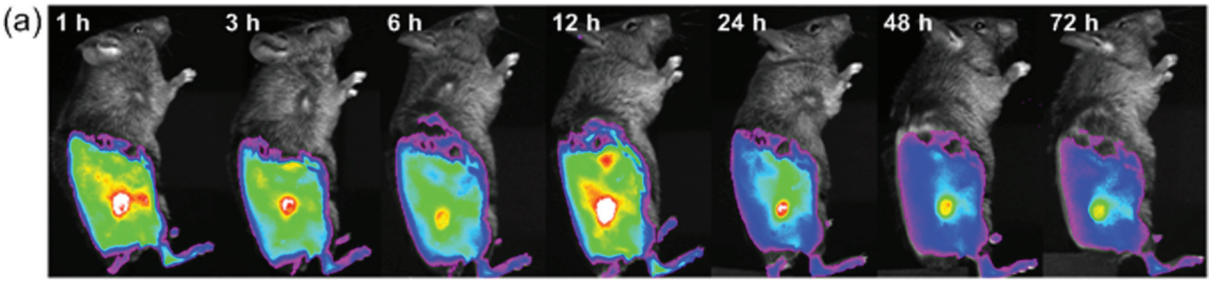

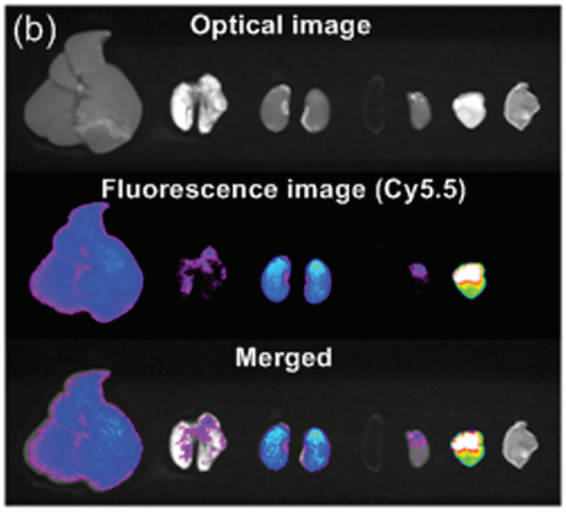

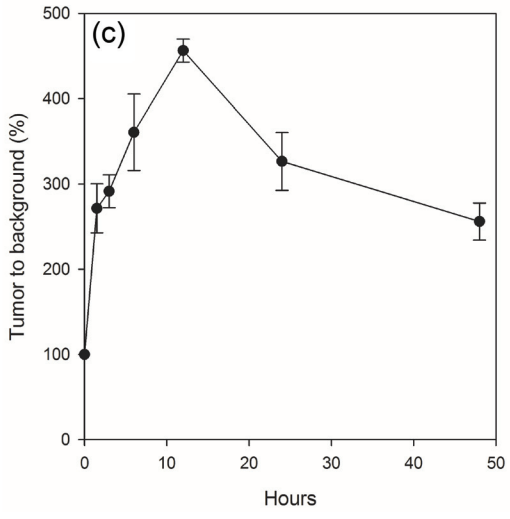

Figure 8. a) Passive targeting ability of the rHG-LA nanoparticle to the tumor region. The rHG-LA nanoparticles were highly accumulated at the tumor region within 1 h and continued to increase up to 12 h. b) Ex vivo observation for organ distribution of the nanoparticles. Major organs, muscle, and tumor were dissected one day after the nanoparticle administration (liver, lung, kidney, spleen, heart, tumor, and muscle; left to right). c) Residence time and elimination of the rHG-LA nanoparticles (data expressed as mean ± S.D.).

to 12 h and subsequently decreased for 72 h. In addition, the tumor-specific accumulation of rHG-LA nanoparticles showed a time-dependent clearance from the site. Taken together, these results indicate that the enhanced anticancer effect of α-TOS via the use of rHG-LA nanoparticles is due to the improved stability of α-TOS in the blood and the increased local concentration of the drug in the tumor region through the EPR effect. The data lead us to conclude that the new strategy to use nanoparticles for the delivery of anticancer agent proposed here is proved and constitutes a promising approach to the cancer nanotherapy.

3. Conclusions

Self-assembled nanoparticles based on rHG conjugated with LA were successfully developed for delivery of α-TOS and the nanoparticles enhanced the cancer-selective anticancer efficacy of α-TOS through improving its stability in physiological conditions and through passive targeting to the tumor. This work demonstrates the dual advantages of passive targeting and cancer cell-selective apoptotic effects over conventional cancer chemotherapy, as well as nanoparticular drug delivery systems that only focus on the passive or active tumor targeting. Although the therapeutic efficacy of the present system needs to be further optimized and the future challenges regarding the immunogenicity of rHG-LA, toxicity in normal tissues, a direct assessment of distribution for α-TOS, and how the nanoparticles protect α-TOS against the hydrolysis remain, the present data demonstrate the promising usefulness of α-TOS/rHG-LA nanoparticles in terms of the dual benefits of passive targeting ability and cancer specificity.

4. Experimental Section

Materials: Recombinant human gelatin (rHG, 100 kDa) was obtained from FibroGen, Inc. (San Francisco, CA). Lipoic acid (LA), alpha-tocopheryl succinate (α-TOS), 1-ethyl-3(3-dimethylaminopropyl) carbodiimide (EDC), *N*-hydroxysuccinimide (NHS), 1,6-diphenyl-1,3,5-hexatriene (DPH), 2, 4, 6-trinitrobenzenesulphonic acid (TNBS), and potassium bromide (KBr, FT-IR grade) were obtained from Sigma-Aldrich Co. (St. Louis, MO). Methanol (HPLC grade) was obtained from Fisher Scientific Korea (Seoul, Republic of Korea). SCC-7 (squamous cell carcinoma), A549 (lung adenocarcinoma), MCF-7 (breast adenocarcinoma), HeLa (cervical carcinoma), and N2A (neuroblastoma) cells were obtained from the American Type Culture Collection (Rockville, MD). Cyanine 5.5 (Cy5.5) was obtained from Amersham Biosciences (Piscataway, NJ).

Preparation of rHG-LA Conjugates: Amphiphilic rHG-LA conjugates were synthesized via EDC/NHS reaction to introduce LA to the hydrophilic rHG backbone through formation of amide bonds, as previously described.[1] To activate the carboxylates, EDC (50 mmol) was added to reaction buffer composed of 60% reaction buffer (0.1 mol MES, 0.5 mol NaCl, pH 6.0) and 40% methanol in the presence of LA (12 mmol). After 30 min, NHS (5 mmol) was added, and the mixture was reacted for 4 h with slow stirring. For EDC inactivation, β-mercaptoethanol was added, and the resulting solution was mixed with 2×PBS (0.2 mol, 0.3 mol NaCl, pH 7.4) containing rHG (5 mg). After 16 h, dialysis was performed to remove impurities. The rHG-LA was lyophilized under vacuum freeze-drying and stored under vacuum at –20 °C until use.

Characterization of rHG-LA Conjugates: The formation of amide bonds between rHG and LA was confirmed using FT-IR, and the remaining amine groups in rHG were quantitatively determined using a TNBS assay. FT-IR spectroscopy was performed using a Nicolet FT-IR spectrometer (Magna-IR 760 ESP, Nicolet Instrument Corp.; Madison, WI). The rHG, LA, and rHG-LA were prepared via grinding with KBr at a ratio of 1:20 and pressing to prepare a thin pellet. In order to determine the remaining amines, sodium bicarbonate (4%, 0.5 mL, pH 8.5) was mixed with each sample (0.5 mL), and freshly prepared, diluted TNBS (0.1%, 0.5 mL) was added. The tightly closed tubes were incubated in the dark at 40 °C for 2 h, and the absorbance at 335 nm was then read using a UV-vis spectrophotometer (SpectraMax M2e, Molecular Devices; Sunnyvale, CA). The blank was prepared according to the identical protocol, using rHG (0.015 to 1 mg mL^{-1}) as the standard.

Critical Aggregation Concentrations (CAC) of rHG-LA Conjugates: A stock solution of DPH (0.4 mmol) in methanol was prepared, and rHG-LA (1 mg mL^{-1} to 1.95 μg mL^{-1}) was dissolved in water with serial dilution. The stock solution of DPH was added to the samples of rHG-LA conjugates (at a final concentration of 0.004 mmol). After sonication at 30% amplification for 20 s, the mixtures were incubated at room temperature for 24 h in the dark. Negative controls were prepared through the same procedure in the absence of DPH. Absorbance of the samples was measured at 356 nm using a UV-vis spectrophotometer (SpectraMax M2e, Molecular Devices; Sunnyvale, CA). The differences in absorbance between the samples with and without DPH were recorded, and CAC was determined based on a significant increase in the absorbance of DPH following incorporation into the rHG-LA nanoparticles.

TEM Analysis and Size Measurements of rHG-LA Nanoparticles: The morphological characteristics of rHG-LA nanoparticles were observed using transmission electron microscopy (TEM; Philips CM-30, Philips Electron Optics; Eindhoven, Netherlands). The rHG-LA was dissolved in water (0.1 mg mL^{-1}) and then dispersed by sonication. One drop of the solution was dried on a carbon grid and stained with osmium tetroxide. The mean diameters of the α-TOS-loaded and unloaded nanoparticles were observed using DLS (Zetasizer Nano ZS, Malvern Instruments Ltd., Malvern, Worcestershire, UK) in autocorrelation mode.

Preparation of α-TOS-Loaded rHG-LA Nanoparticles: A co-solvent to dissolve both rHG-LA and α-TOS is necessary for loading α-TOS into the hydrophobic core of rHG-LA nanoparticles. The conjugates of rHG-LA (2 mg mL^{-1}) and α-TOS (0.2 mg mL^{-1}) were separately dissolved in DMSO, and the rHG-LA was sonicated at 30% amplification for 20 s. DMSO containing α-TOS was mixed with the rHG-LA at a volume ratio of 1:1. The mixture was sonicated again under the same conditions, and the resulting mixture was dialyzed (molecular weight cutoff (MWCO) 1 kDa) against water for 9 h. After dialysis, the α-TOS-loaded rHG-LA nanoparticles were freeze-dried and stored under vacuum at –20 °C until use. The loading efficiency (LE) and loading contents (LC) of α-TOS in rHG-LA nanoparticles were determined using HPLC (1525 dual pump, Waters; Milford, MA) equipped with a UV-detector set at 290 nm and a C18 column. The mobile phase was a mixture of methanol (95%) and water (5%), and the samples were eluted with mobile phase in an isocratic mode at a flow rate of 1 mL min^{-1}. LC% and LE% were calculated as: LC% = mass of α-TOS in nanoparticles/mass of α-TOS-loaded nanoparticles × 100, and, LE% = mass of α-TOS loaded in nanoparticles/mass of α-TOS added × 100.

Stability of α-TOS-Loaded rHG-LA Nanoparticles: The stability of the nanoparticles was examined in both salt- and HSA-containing solutions. The nanoparticles were dispersed in PBS (pH 7.4, 0.1 mg mL^{-1}) and the size and zeta potential were measured. To examine the nanoparticle stability in the presence of serum protein, a dispersion of nanoparticles in PBS (1 mg mL^{-1}) and HSA solution (PBS, 22 mg mL^{-1}) were mixed at a ratio of 1:10 (v/v). The size and zeta potential were measured for 6 h at 12 min intervals.

In Vitro Release of α-TOS from the rHG-LA Nanoparticles: A dispersion of α-TOS-loaded rHG-LA nanoparticles was prepared in PBS (3 mg mL^{-1}) and placed in a dialysis bag (MWCO 1 kDa), which was immersed into PBS (20 mL) in a conical tube. The conical tube was placed in a shaking water bath at 37 °C. The incubated dialysate was collected at predetermined time points and was replaced with fresh PBS (20 mL). The α-TOS released was quantified using HPLC as described above.

Cell Culture: RPMI 1640 was used for SCC (squamous cell carcinoma), A549 (lung adenocarcinoma), and MCF-7 (breast adenocarcinoma)

cell lines, and DMEM was selected for Hela (cervical cancer), N2A (neuroblastoma), and normal cell lines (H9C2, 3T3L1 and HEK293). The media both contained FBS (10%) and penicillin-streptomycin (1%). The cells were cultured to 80% confluence at 37 °C with 5% CO_2.

Cellular Uptake of rHG-LA Nanoparticles: The rHG-LA nanoparticles were labeled with NHS-Cy5.5 according to the manufacturer's instructions. SCC cells were seeded onto 60 mm dishes at a density of 1×10^6 cells dish^{-1}. After 24 h of incubation, the Cy5.5-rHG-LA nanoparticles were added to the dish (50 μg mL^{-1}). The cells were washed three times with PBS at the predetermined time points. Cell nuclei were counterstained with DAPI, and cell morphologies were visualized in differential interference contrast (DIC) images. The intracellular localization of rHG-LA nanoparticles was observed using confocal laser scanning microscopy (CLSM, LSM510 META NLO; Carl Zeiss Jena GmbH, Germany) at the Korea Basic Science Institute, Chuncheon Center (Chuncheon, Korea). The cellular uptake of rHG-LA nanoparticles was quantitatively analyzed using a FACSCalibur (BD Biosciences, San Jose, CA).

In Vitro Anticancer Effects of α-TOS-Loaded rHG-LA Nanoparticles: The cancer cell-specific apoptotic effects of α-TOS-loaded nanoparticles were examined in five cancer cell lines (SCC, A549, MCF-7, Hela, and N2A) and three normal cell lines (H9C2 (cardiomyoblast), 3T3-L1 (fibroblast), and HEK293 (human embryonic kidney 293)). The cells were treated with α-TOS-loaded rHG-LA nanoparticles, non-loaded rHG-LA nanoparticles, and free α-TOS at various concentrations (0–25 μg mL^{-1}). The cancer cell-selective apoptotic effects of the nanoparticles were investigated by measuring viabilities in those cell lines, which were determined using the MTT assay following incubation for 48 h.

Tumor Model: SCC cells were trypsinized and suspended in plain media at a density of 3.0×10^7 cells mL^{-1}. Fifty microliters of the cell suspension were injected subcutaneously into the left hind flanks of six-week-old C3H mice (20 to 25 g). The tumor volume was measured using a caliper and calculated using the formula $V = ab^2/2$, where a and b are the longest and shortest dimensions, respectively.

In Vivo Antitumor Effects of α-TOS-Loaded rHG-LA Nanoparticles: The tumor model was prepared as described above, and the mice were randomly divided into test groups when the tumor volumes reached approximately 70 mm^3. The α-TOS-loaded nanoparticles were injected into the tail veins of the tumor-bearing mice (10 mg kg^{-1}). The treated group was divided into four groups of five mice each, which were treated further with i) saline, ii) non-loaded rHG-LA nanoparticles, iii) α-TOS-loaded rHG-LA nanoparticles (10 mg α-TOS kg^{-1}), and, iv) free α-TOS (10 mg kg^{-1}). These treatments were repeated every three days.

Tumor-Targeting Ability of rHG-LA Nanoparticles: When tumor volumes approached approximately 200 mm^3, the Cy5.5-labeled rHG-LA nanoparticles were injected intravenously into the mice. The tumor-targeting ability of the nanoparticles was visualized and quantitatively analyzed using a fluorescence intensity detector with an imaging station (Kodak Image Station 4000MM, Eastman Kodak Company, Scientific Imaging Systems; New Haven, CT) at predetermined time points. Tumors and major organs, including liver, lung, kidney, spleen, and heart, were dissected 12 h after intravenous injection of Cy5.5-labeled rHG-LA nanoparticles. The distribution of rHG-LA nanoparticles in the organs and tumors was quantitatively analyzed.

Acknowledgements

Y.-W.W. and S.-M.Y. contributed equally to this work. This work was partially supported by grants from the Korea Science and Engineering Foundation (2011K000963, 2011K000803) and World Class University program (WCU, R332010000100360) through the National Research Foundation of Korea funded by the Ministry of Education, Science, and Technology and Seoul R&BD Program (ST100071M093212).

Received: August 22, 2011
Revised: November 21, 2011
Published online: January 18, 2012

[1] H.-Y. Hwang, I.-S. Kim, I. C. Kwon, Y.-H. Kim, *J. Controlled Release* **2008**, *128*, 23.
[2] L. L. Ma, P. Jie, S. S. Venkatraman, *Adv. Funct. Mater.* **2008**, *18*, 716.
[3] M. Shi, K. Ho, A. Keating, M. S. Shoichet, *Adv. Funct. Mater.* **2009**, *19*, 1689.
[4] H. Maeda, G. Y. Bharate, J. Daruwalla, *Eur. J. Pharm. Biopharm.* **2009**, *71*, 409.
[5] C. K. Huang, C. L. Lo, H. H. Chen, G. H. Hsiue, *Adv. Funct. Mater.* **2007**, *17*, 2291.
[6] S. Cai, S. Thati, T. R. Bagby, H.-M. Diab, N. M. Davies, M. S. Cohen, M. L. Forrest, *J. Controlled Release* **2010**, *146*, 212.
[7] K. Cho, X. Wang, S. Nie, Z. Chen, D. M. Shin, *Clin. Cancer Res.* **2008**, *14*, 1310.
[8] J. D. Byrne, T. Betancourt, L. Brannon-Peppas, *Adv. Drug Delivery Rev.* **2008**, *60*, 1615.
[9] Q. X. Li, D. H. Yu, G. Liu, N. Ke, J. McKelvy, F. Wong-Staal, *Cell Death Differ.* **2008**, *15*, 1197.
[10] K. N. Prasad, B. Kumar, X.-D. Yan, A. J. Hanson, W. C. Cole, *J. Am. Coll. Nutr.* **2003**, *22*, 108.
[11] L.-F. Dong, V. J. A. Jameson, D. Tilly, L. Prochazka, J. Rohlena, K. Valis, J. Truksa, R. Zobalova, E. Mahdavian, K. Kluckova, M. Stantic, J. Stursa, R. Freeman, P. K. Witting, E. Norberg, J. Goodwin, B. A. Salvatore, J. Novotna, J. Turanek, M. Ledvina, P. Hozak, B. Zhivotovsky, M. J. Coster, S. J. Ralph, R. A. J. Smith, J. Neuzil, *Free Radic. Biol. Med.* **2011**, *50*, 1546.
[12] P. W. Sylvester, in *Vitamins & Hormones*, Vol. *76*, (Ed: G. Litwack), Academic Press, New York **2007**, 329.
[13] V. Gogvadze, E. Norberg, S. Orrenius, B. Zhivotovsky, *Int. J. Cancer* **2010**, *127*, 1823.
[14] T. Weber, H. Dalen, L. Andera, A. Nègre-Salvayre, N. Augé, M. Sticha, A. Lloret, A. Terman, P. K. Witting, M. Higuchi, M. Plasilova, J. Zivny, N. Gellert, C. Weber, J. Neuzil, *Biochemistry* **2003**, *42*, 4277.
[15] J. Neuzil, K. Kågedal, L. Andera, C. Weber, U. T. Brunk, *Apoptosis* **2002**, *7*, 179.
[16] Y.-W. Won, Y.-H. Kim, *J. Controlled Release* **2008**, *127*, 154.
[17] M. Jahanshahi, M. H. Sanati, S. Hajizadeh, Z. Babaei, *Phys. Status Solidi A* **2008**, *205*, 2898.
[18] Y.-W. Won, Y.-H. Kim, *Macromol. Res.* **2009**, *17*, 464.
[19] S. Young, M. Wong, Y. Tabata, A. G. Mikos, *J. Controlled Release* **2005**, *109*, 256.
[20] D. Olsen, J. Jiang, R. Chang, R. Duffy, M. Sakaguchi, S. Leigh, R. Lundgard, J. Ju, F. Buschman, V. Truong-Le, B. Pham, J. W. Polarek, *Protein Expression Purif.* **2005**, *40*, 346.
[21] A. Gupte, R. J. Mumper, *Cancer Treat. Rev.* **2009**, *35*, 32.
[22] L. Packer, E. H. Witt, H. J. Tritschler, *Free Radic. Biol. Med.* **1995**, *19*, 227.
[23] F. Cavalieri, A. Postma, L. Lee, F. Caruso, *ACS Nano* **2009**, *3*, 234.
[24] H. Zhou, W. Yu, X. Guo, X. Liu, N. Li, Y. Zhang, X. Ma, *Biomacromolecules* **2010**, *11*, 3480.
[25] M. Barzegar-Jalali, K. Adibkia, H. Valizadeh, M. Shadbad, A. Nokhodchi, Y. Omidi, G. Mohammadi, S. Nezhadi, M. Hasan, *J. Pharm. Pharm. Sci.* **2008**, *11*, 167.
[26] A. Khan, M. I. Khan, Z. Iqbal, Y. Shah, L. Ahmad, D. G. Watson, *J. Chromatogr. B* **2010**, *878*, 2339.
[27] Q. Su, K. G. Rowley, K. O'Dea, *J. Chromatogr. B* **1999**, *729*, 191.
[28] C. Constantinou, A. Papas, A. I. Constantinou, *Int. J. Cancer* **2008**, *123*, 739.
[29] X. Gu, X. Song, Y. Dong, H. Cai, E. Walters, R. Zhang, X. Pang, T. Xie, Y. Guo, R. Sridhar, J. A. Califano, *Clin. Cancer Res.* **2008**, *14*, 1840.
[30] Y.-W. Won, S.-M. Yoon, C. H. Sonn, K.-M. Lee, Y.-H. Kim, *ACS Nano* **2011**, *5*, 3839.